Three-dimensional metamaterial Hall-bar devices

Christian Kern* and Martin Wegener
Institute of Applied Physics, Karlsruhe Institute of Technology (KIT), 76128 Karlsruhe, Germany
and Institute of Nanotechnology, Karlsruhe Institute of Technology (KIT), 76021 Karlsruhe, Germany

(Received 24 September 2018; published 28 January 2019)

We realize classical Hall bars, made of chain-mail-inspired cubic-symmetry 3D metamaterials composed of interlinked hollow tori, contacted to printed circuit boards. This step is a prerequisite for refined experiments compared to our previous probe-station based measurements as well as for potential applications of 3D Hall-effect metamaterials in general. On this basis, we systematically study the dependence of the Hall voltage on the relative orientation of the 3D metamaterial crystallographic axes with respect to the applied static magnetic field vector and the imposed current flow direction. Our findings are consistent with an isotropic sign-reversed Hall coefficient, which has been predicted by homogenization theory.

DOI: 10.1103/PhysRevMaterials.3.015204

I. INTRODUCTION

Studies on the magnetotransport of charge carriers in crystals such as Si, GaAs/AlGaAs heterostructures, or graphene have led to a wealth of physical phenomena [1–3]. Yet richer behavior can be found in materials that are intentionally micro- or nanostructured to form potential landscapes, which can be seen as artificial two-dimensional (2D) or three-dimensional (3D) crystals. Such man-made crystals have, e.g., led to the experimental observation [4–6] of the Hofstadter butterfly [7] in high-mobility van-der-Waals heterostructures at low temperatures. Weiss oscillations on GaAs/AlGaAs heterostructures have been a precursor [8]. Square arrays of cylindrical voids in a layer of bulk GaAs have led to an unusual highly anisotropic effective magnetoresistance [9]. Artificial crystals in presence of a strong magnetic field can perhaps increase the dimensionless effective ZT value of thermoelectrics [10]. Furthermore, the sign of the isotropic effective Hall coefficient in 3D artificial crystals can be different from that of the constituent materials [11,12]. Finally, the effective isotropic Hall mobility of a 3D artificial crystal can conceptually be larger than the Hall mobility of all constituents [13].

Today, rationally designed artificial crystals are referred to as "metamaterials" if one can assign effective-medium parameters to them which go beyond ("meta") those of their bulk ingredient materials. The effective metamaterial properties are mainly determined by micro- or nanostructure, which makes them amenable to predictable and controlled manipulation. As an extreme example, the sign of certain effective metamaterial parameters (e.g., electric permittivity, mechanical compressibility, or Hall coefficient) can be reversed with respect to the sign of the ingredient-materials' parameters. Some effective parameters can even be conceptually unbounded [14]. While many electromagnetic/optical [15,16] and acoustic/mechanical [17–19] metamaterial properties have been investigated, a much smaller number of studies has targeted the magnetotransport of charge carriers.

Our early experimental work on Hall-effect metamaterials at room temperature was in the regime of small charge-carrier mobilities (and magnetic flux densities of $B \approx 1$ T, leading to small values of the product of mobility and magnetic flux density, $\mu B \ll 1$). The chainmail-inspired metamaterial crystals were composed of interlinked hollow ZnO tori. For convenience of the reader, an illustration of this artificial crystal is reproduced in Fig. 1 [20].

Our measurements on such 3D artificial crystals showed a reversal of the Hall voltage with respect to the Hall voltage of the single ingredient bulk ZnO semiconductor [20] (in air/vacuum). The origin of this sign reversal could later be traced back to the topology of the involved tori in the unit cell and is related to so-called anti-Hall bars [21–23]. In the process of discussing this connection, doubts were expressed that the observed sign reversal of the Hall voltage can actually be interpreted in terms of the sign reversal of the Hall coefficient of an effective medium or material [22]. From the viewpoint of homogenization theory [13], the situation is clear. The cubic crystal symmetry guarantees an isotropic scalar effective metamaterial Hall coefficient, which is sign inverted with respect to the constituent material Hall coefficient [13]. However, the important aspect of isotropy has not yet been demonstrated in direct experiments.

All of these 3D microstructured metamaterials were made by 3D optical laser lithography [24] of a polymer scaffold and subsequent atomic-layer deposition of a thin ZnO film onto this electrically insulating scaffold. So far, however, measurements on these samples have been restricted to a dedicated magnetoelectric probe station, because electrically contacting these artificial 3D crystals in a permanent manner has been a major technological hurdle. The use of a probe station required regular readjustment of the four contact needles and led to limited sample lifetimes.

In this paper, we describe a fabrication route allowing for contacting 3D-metamaterial-based Hall bars to printed circuit boards. This technological novelty of our work is an obvious

*christian.kern@kit.edu

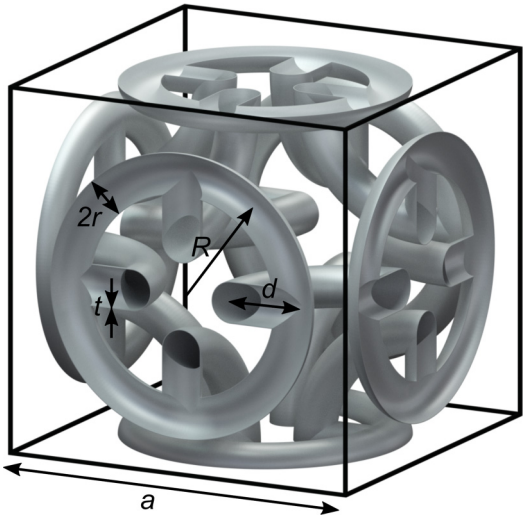

FIG. 1. Illustration of the 3D metamaterial crystal unit cell. The cubic lattice constant a, the major torus radius R, the minor torus radius r, the distance parameter d, and the thickness t of the semiconductor layer are indicated. Adapted with permission from Ref. [20].

prerequisite for potential future applications [25]. In addition, it allows us to readily perform previously cumbersome experiments, which forms a second novelty of our work: we investigate the dependence of the Hall voltage on the relative orientation of the metamaterial crystallographic axes with respect to the applied static magnetic field vector and the imposed current flow direction. These data provide evidence that our experiments in Ref. [20] and in this paper can indeed be interpreted in terms of a sign reversal of the *isotropic* effective metamaterial Hall coefficient.

II. FABRICATION

Different steps of the four-contact metamaterial Hall-bar fabrication process are illustrated in Fig. 2. For each sample, our fabrication starts with 3D dip-in laser lithography (Photonics Professional GT, Nanoscribe GmbH) of a polymer scaffold (IP-S, Nanoscribe GmbH) on a silicon substrate using a 25 × NA 0.8 objective. This electrically insulating polymer scaffold includes an elongated arm with a rectangular cross section of 50 μm × 100 μm and a length of 1 mm for later manual handling and four pedestals. By using atomic-layer deposition (ALD), the entire structure is subsequently conformally coated with an n-type ZnO semiconductor film. We deposit 1000 ALD cycles of ZnO from diethylzinc and water at a substrate temperature of 200 °C and at an Ar flow of 20 sccm using a commercial ALD system (Savannah 100, Cambridge Nanotech, Inc.). This ZnO layer has a thickness of 0.17 μm, as determined by ellipsometry on silicon substrates. It has a negative Hall coefficient of $A_H = -3.02 \times 10^{-7}$ m^3 A^{-1}s^{-1}, as measured on the unstructured ZnO film on a glass substrate (with the thin Al_2O_3 layer mentioned below) in a van-der-Pauw geometry. Next, we manually dispense electrically conductive epoxy resin (EC 101, Polytec PT GmbH) using a syringe with a dispense tip with an inner diameter of 150 μm and a stereo microscope

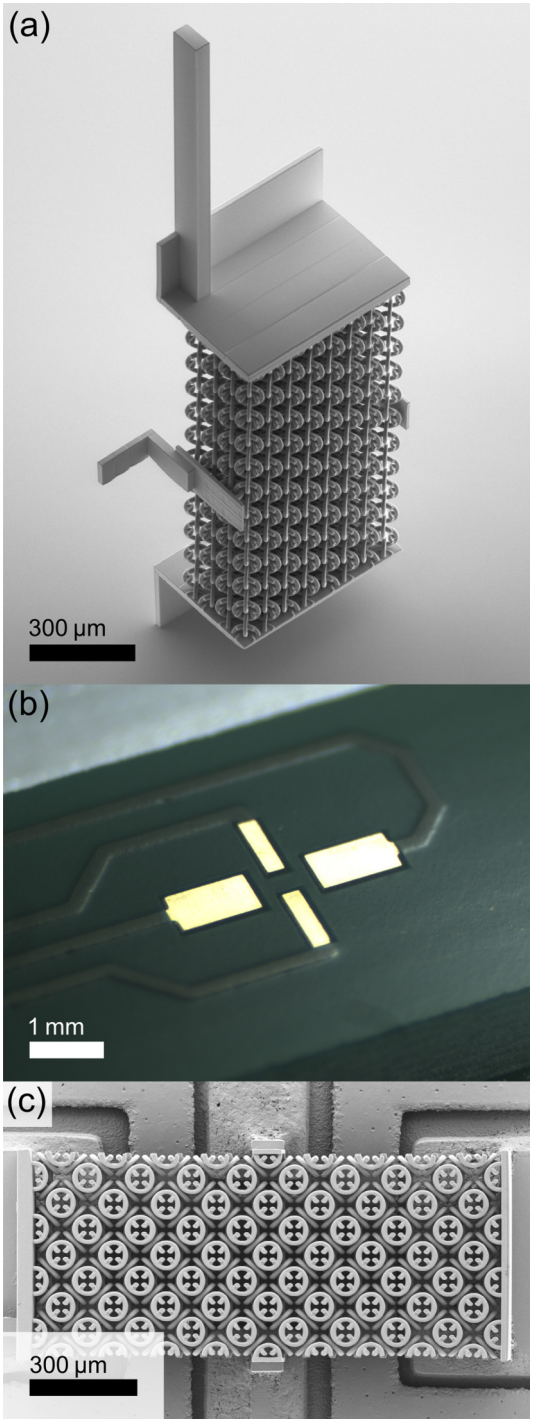

FIG. 2. Metamaterial Hall-bar samples in different stages of fabrication. (a) Scanning electron micrograph of a Hall-bar on a silicon substrate after 3D laser lithography and ALD, before transfer of the structure. The structure includes a handling arm (on top) and four pedestals. The unit cell orientation corresponds to case D (compare Fig. 3). (b) Optical image of the printed circuit board with four contact pads featuring an electroless nickel immersion gold (ENIG) surface plating. (c) Scanning electron micrograph of a sample on a printed circuit board after transfer and curing of the conductive epoxy. The unit cell orientation corresponds to case C (compare Fig. 3). The geometrical target parameters (compare Fig. 1) for all samples are $a = 104$ μm, $R = 36$ μm, $r = 6$ μm, $d = -20$ μm, and $t = 0.17$ μm.

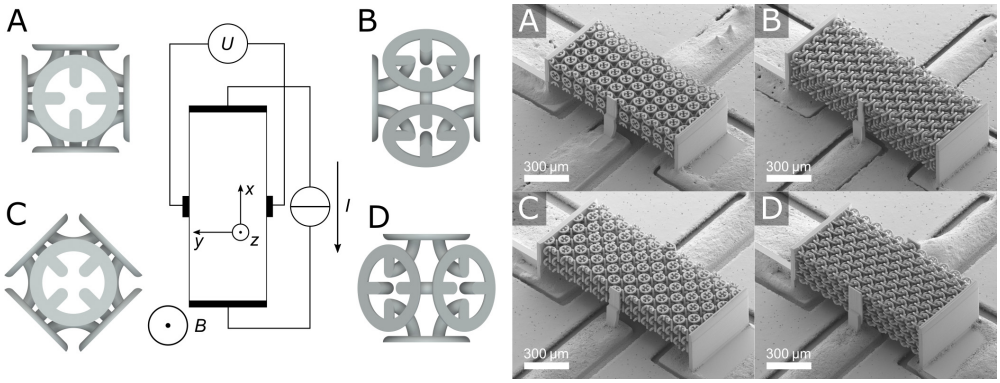

FIG. 3. (Left) Schematic representation of the four different unit-cell orientations A-D with respect to the Hall bar that were studied experimentally (compare Fig. 1). (Right) Scanning electron micrographs of the corresponding metamaterial Hall-bar samples. Results for the four orientations A-D are shown in Fig. 4 and are summarized in Table I.

on four contact pads of a prefabricated printed circuit board. Thereafter, by means of a scalpel, we carefully mechanically break the structure off the silicon substrate at its bottom. By manipulating the sample via the handling arm using a pair of fine-tip tweezers and a stereo microscope, we position it onto the printed circuit board. In the final step, the conductive epoxy resin is cured at 125 °C for 25 minutes on a hotplate. Electrical contact to the measurement instrumentation (see below) is made by a standard box header connector, which is soldered onto the printed circuit board. Notably, the reverse sequence (i.e., sample transfer first and then ALD coating) is not possible because the ALD process in this case also conformally coats all surfaces, including the circuit board, leading to short circuits. In principle, one might consider a selective passivation of the surfaces with respect to the ALD growth of ZnO. Indeed, such passivation has been reported in the literature [26]. However, we have not succeeded in obtaining a reliable passivation for comparably thick ZnO layers without affecting the growth in the vicinity of the passivating layer.

The manual handling of the samples is amazingly reproducible. The most critical step is rather the ALD. We have found that the growth of ZnO is affected in the vicinity of the polymer template, leading to spatially inhomogeneous deposition, even after conformally depositing a thin base layer of Al_3O_2 (50 ALD cycles grown from trimethylaluminum and water at 150 °C), onto the polymer structures. In extreme cases, halos appear on the substrate around the metamaterial Hall bar. These issues have been mostly resolved by using, in addition to the Al_3O_2 layer, an optimized development process, and a baking step (7 hours at 200 °C temperature) in the ALD chamber before the actual deposition. In the optimized development process, the polymer templates are immersed in a commercial solvent-based developer (mr-Dev 600, contains 1-Methoxy-2-propanyl acetate, micro resist technology GmbH) for 60 minutes and subsequently in isopropyl alcohol and water for 2 minutes each. We have avoided the use of acetone in the development process, as it led to more pronounced inhomogeneities in early sample generations. This observation seems to be related to the swelling of IP-S microstructures in acetone. For reasons unclear to us, we have not observed these issues previously [20]. Nevertheless and despite of these measures, certain relative variations of the extracted Hall coefficients for nominally identical samples on the order of ±7% have remained (see below). We have observed similar variations for nominally identical plain ZnO films grown by ALD on silicon substrates.

III. EXPERIMENTAL RESULTS

To demonstrate that these samples are functioning and that they allow for going beyond our previous probe-station based measurements, we now discuss a series of cubic-symmetry samples, aiming at investigating the isotropy of the 3D metamaterial Hall effect. As discussed in Ref. [13], only rotating the magnetic field with respect to a given sample is not sufficient. One also has to change the direction of current flow with respect to the crystallographic axes to investigate the isotropy of the effective Hall coefficient. We consider the previously introduced chainmail-inspired metamaterial for negative distance parameters d leading to a sign-inversion of the effective Hall coefficent. It has been shown that cubic crystal symmetry, which is characterized by four threefold symmetry axes, always leads to an effectively isotropic (scalar) Hall coefficient rather than to a generally anisotropic Hall tensor for lower crystal symmetries [13]. However, these strict results are based on the assumption of infinitely extended 3D periodic structures without any contacts. Actual Hall bars are rather finite along all three spatial directions and necessarily contain four contacts, which also disturb the local potentials and hence the Hall voltage [27]. In principle, one should investigate infinitely many unit cell orientations. In our experiments, we vicariously consider four different metamaterial crystal orientations A-D (see Fig. 3). In our original work, the magnetic flux density vector $\vec{B}$, the current flow direction, and the pick-up direction of the Hall voltage were all along the three principal cubic axes (orientation A in Fig. 3). In the additional three cases B-D, two of these directions are along cubic face diagonals of the structure. We measure the conventional, orthogonal Hall voltages of sample geometries A-D. We investigate two samples for each geometry.

Clearly, these choices A-D inherently lead to different sample surface terminations. As all surfaces are coated

TABLE I. Summary of the four different sample geometries A-D (compare Fig. 3). The first three rows list the outer dimensions, L_x, L_y, and Lz, of the cuboid metamaterial Hall bars in units of the cubic lattice constant, $a = 104$ μm. The last two rows give the experimentally determined effective Hall coefficients A_H^* in units of the Hall coefficient of the unstructured ZnO films, A_H^0 for two different sample generations. These values can be compared to theory. Numerical calculations (see Ref. [13]) for the geometrical target parameters given in the caption of Fig. 2, for an infinitely extended 3D metamaterial crystal, and without contacts yield $A_H^* = -100A_H^0$.

	A	B	C	D
L_x/a	11	$9\sqrt{2}$	$9\sqrt{2}$	11
L_y/a	5	5	$4\sqrt{2}$	$4\sqrt{2}$
L_z/a	2	$2\sqrt{2}$	2	$2\sqrt{2}$
A_H^*/A_H^0	−65	−70	−67	−76
A_H^*/A_H^0	−74	−67	−58	−68

conformally, these terminations are chosen carefully, such that the influence of the ALD coating on the outer surfaces is minimized. Furthermore, the outer dimensions L_x, L_y, and L_z of the cuboid Hall bars (of course not including the handling arm and the pedestals, compare Fig. 2) are slightly different (see Table I). The effect of different sample thicknesses L_z along the magnetic field direction will be considered in the analysis below. Imperfections arise due to 3D laser lithography from the elongated shape of the focal volume (the "voxel"). As the torus cross section is composed of many voxels, this asymmetry is reduced. Nevertheless, this aspect leads to small deviations from the targeted geometry. More precisely, slightly ellipsoidal cross sections of the polymer tori and cylinders remain.

As in all Hall measurements, the quality of the contacts is very important. In principle, the contacts do not need to have Ohmic characteristics. However, they should allow for imposing the desired current flow and be sufficiently stable. Furthermore, non-Ohmic behavior can lead to rectification of ac noise [28]. Previously, we have used a bilayer of titanium and gold leading to excellent Ohmic behavior [20,29]. Here, we directly contact the ZnO with the electrically conductive epoxy resin. These contacts exhibit small deviations from the ideal behavior. We characterize the contacts by measuring the I-V curve for each pair of contacts. The resistances, as obtained from fits to these I-V curves, are on the order of 2 kΩ. For the large current-injection contacts, the relative deviation of the current from these fits is below 1%. However, for the two smaller pick-up contacts the deviation becomes as large as 17%.

Measurements according to the scheme shown on the left of Fig. 3 were performed by imposing a constant current flow I and measuring the corresponding transversal voltage using a source-measurement unit (B2901A, Keysight Technologies, Inc.). The magnetic flux density, $B_z = \pm 0.83$ T, was imposed using a permanent magnet (see Ref. [20]) and can be inverted by a 180° rotation of the magnet. For this rotation, the width of the circuit board of 6 mm has to be smaller than the gap size of the magnet (15 mm). In a single measurement, the

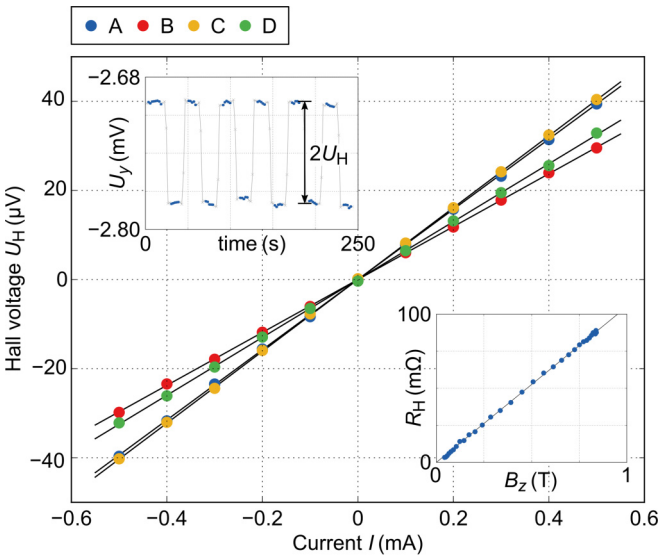

FIG. 4. Measured Hall voltage U_H vs electric current I for four different Hall-bar samples corresponding to the four different unit-cell orientations A-D illustrated in Fig. 3. The dots are measured, the straight lines are guides the eye. The slope of the straight lines is the Hall resistance R_H. In the ideal case of an isotropic Hall coefficient and identical sample thicknesses L_z, the slopes should be identical. Due to the different sample thicknesses L_z (compare Table I), the slopes of the pairs (A,C) and (B,D) are slightly different. The upper inset shows raw data for case A, current $I = 0.5$ mA, and a magnetic flux density $B_z = \pm 0.83$ T. The lower inset is an example measurement of R_H versus B_z for $I = 0.5$ mA and sample type A, showing the expected proportional behavior. Here, B_z has been varied by changing the position of the magnet with respect to the sample. The relation between position and B_z has been determined by a calibration measurement using a standard Hall sensor. All of the derived effective Hall coefficients $A_H^* = R_H L_z/B_z$ are summarized in the fourth row of Table I. The fifth row there corresponds to a second generation of nominally identical samples A-D.

magnetic field is flipped repeatedly (see upper inset in Fig. 4). Performing such measurements for eleven different values of the electric current I results in the anticipated proportional behavior $U_H = R_H I$ shown in Fig. 4. The Hall resistance, R_H, is proportional to the magnetic flux density. As an example, the lower inset in Fig. 4 shows the measured R_H versus B_z for sample type A and fixed I.

For each of the devices A-D (compare Fig. 3), R_H is given by the slope of U_H versus I for fixed $B_z = 0.83$ T. We extract the effective metamaterial Hall coefficient from the relation $A_H^* = R_H L_z/B_z$. As pointed out above, L_z is different for the four different metamaterial crystal orientations A-D (compare Fig. 3). The values for L_z are summarized in the first three rows of Table I. The last two rows summarize the derived values for A_H^* for two different sample generations.

Most importantly, the resulting values of A_H^* are all sign-inverted with respect to A_H^0. Their modulus is much larger than than the Hall coefficient of the ZnO reference films A_H^0. This aspect is simply due to the confinement of the current to a thin layer [13]. All values of the effective Hall coefficient are the same within ±13%. This finding is consistent with the theoretically expected isotropy of the Hall effect.

As discussed in the sample fabrication above, we attribute the remaining variations among nominally identical samples mainly to the ALD process. Variations between samples with different unit cell orientations have a number of additional causes. As mentioned, these samples vary in surface termination and outer dimensions (implying different contact sizes). Furthermore, variations may arise from the aforementioned asymmetries caused by the 3D laser lithography process. Finally, one should keep in mind that truly identical behavior independently of unit cell orientation is only expected for samples composed of infinitely many unit cells.

IV. CONCLUSIONS

In conclusion, we have experimentally realized microscale 3D metamaterial Hall-bar devices integrated on printed circuit boards. This novel approach goes beyond our previous probe-station based experiments. On this basis, we have investigated the orientation dependence of the sign-inverted effective Hall effect of cubic-symmetry 3D metamaterials composed of interlinked hollow semiconductor tori. Our findings are consistent with an isotropic effect, in agreement with theory. The same fabrication approach can be used for lower-symmetry Hall-effect metamaterials, for which we have previously suggested potential applications in terms of measuring directly the local circulation of the magnetic field [25].

ACKNOWLEDGMENTS

We acknowledge support by the Karlsruhe School of Optics and Photonics (KSOP), the Hector Fellow Academy, the KIT Nanostructure Service Laboratory (NSL), and the Helmholtz Program Science and Technology of Nanosystems (STN). We thank Muamer Kadic, Andreas Fischer, Jessica Meier, Markus Zieger, Eva Blasco (all KIT or formerly KIT), and Alexander Quick (Nanoscribe GmbH) for helpful discussions. Furthermore, we thank Andreas Wickberg (KIT) for help regarding the ALD, Andreas Wickberg, and Tobias Frenzel (KIT) for taking the scanning electron micrographs, and Jurana Hetterich and Adrian Mertens (both KIT) for the ellipsometry measurements.

[1] K. v. Klitzing, G. Dorda, and M. Pepper, Phys. Rev. Lett. **45**, 494 (1980).
[2] D. C. Tsui, H. L. Störmer, and A. C. Gossard, Phys. Rev. Lett. **48**, 1559 (1982).
[3] K. S. Novoselov, Z. Jiang, Y. Zhang, S. Morozov, H. L. Stormer, U. Zeitler, J. Maan, G. Boebinger, P. Kim, and A. K. Geim, Science **315**, 1379 (2007).
[4] B. Hunt, J. Sanchez-Yamagishi, A. Young, M. Yankowitz, B. J. LeRoy, K. Watanabe, T. Taniguchi, P. Moon, M. Koshino, P. Jarillo-Herrero *et al.*, Science **340**, 1427 (2013).
[5] C. R. Dean, L. Wang, P. Maher, C. Forsythe, F. Ghahari, Y. Gao, J. Katoch, M. Ishigami, P. Moon, M. Koshino *et al.*, Nature (London) **497**, 598 (2013).
[6] L. Ponomarenko, R. Gorbachev, G. Yu, D. Elias, R. Jalil, A. Patel, A. Mishchenko, A. Mayorov, C. Woods, J. Wallbank *et al.*, Nature (London) **497**, 594 (2013).
[7] D. R. Hofstadter, Phys. Rev. B **14**, 2239 (1976).
[8] D. Weiss, K. Klitzing, K. Ploog, and G. Weimann, Europhys. Lett. **8**, 179 (1989).
[9] M. Tornow, D. Weiss, K. v. Klitzing, K. Eberl, D. J. Bergman, and Y. M. Strelniker, Phys. Rev. Lett. **77**, 147 (1996).
[10] Y. M. Strelniker and D. J. Bergman, Phys. Rev. B **96**, 235308 (2017).
[11] M. Briane, G. W. Milton, and V. Nesi, Arch. Ration. Mech. Anal. **173**, 133 (2004).
[12] M. Briane and G. W. Milton, Arch. Ration. Mech. Anal. **193**, 715 (2009).
[13] C. Kern, G. W. Milton, M. Kadic, and M. Wegener, New J. Phys. **20**, 083034 (2018).
[14] M. Briane and G. W. Milton, Multiscale Model. Simul. **7**, 1405 (2009).
[15] C. Caloz and T. Itoh, *Electromagnetic Metamaterials: Transmission Line Theory and Microwave Applications* (Wiley, Hoboken, NJ, 2005).
[16] C. M. Soukoulis and M. Wegener, Nat. Photon. **5**, 523 (2011).
[17] R. V. Craster and S. Guenneau, *Acoustic Metamaterials: Negative Refraction, Imaging, Lensing and Cloaking* (Springer Science & Business Media, Dordrecht, 2012).
[18] G. Ma and P. Sheng, Sci. Adv. **2**, e1501595 (2016).
[19] J. Christensen, M. Kadic, O. Kraft, and M. Wegener, MRS Commun. **5**, 453 (2015).
[20] C. Kern, M. Kadic, and M. Wegener, Phys. Rev. Lett. **118**, 016601 (2017).
[21] R. G. Mani and K. von Klitzing, Appl. Phys. Lett. **64**, 1262 (1994).
[22] J. Oswald, Phys. Rev. Lett. **120**, 149701 (2018).
[23] C. Kern, M. Kadic, and M. Wegener, Phys. Rev. Lett. **120**, 149702 (2018).
[24] G. von Freymann, A. Ledermann, M. Thiel, I. Staude, S. Essig, K. Busch, and M. Wegener, Adv. Funct. Mater. **20**, 1038 (2010).
[25] C. Kern, V. Schuster, M. Kadic, and M. Wegener, Phys. Rev. Appl. **7**, 044001 (2017).
[26] A. Mackus, A. Bol, and W. Kessels, Nanoscale **6**, 10941 (2014).
[27] R. S. Popovic, *Hall Effect Devices* (Taylor & Francis, London, 2003).
[28] *Low Level Measurements Handbook*, 7th ed. (Keithley, Tektronix, 2014).
[29] L. J. Brillson and Y. Lu, J. Appl. Phys. **109**, 8 (2011).